A Reaction-Diffusion Model of the Centromere-Signaling Network
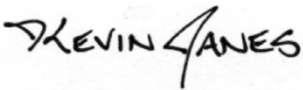
A Technical Report

in STS 4600

Presented to

The Faculty of the

School of Engineering and Applied Science

University of Virginia

In Partial Fulfillment of the Requirements for the Degree

Bachelor of Science in Biomedical Engineering

Lydia Erbaugh
May 4, 2020

Technical Project Team Members:
Jasraj Raghuwanshi

approved: _____ date: _____
Dr. Kevin Janes, Department of Biomedical Engineering

approved: _____ date: _____
Dr. Todd Stukenberg, Department of Biochemistry and Molecular Genetics

Abstract

The centromere-signaling network (CSN) consists of two positive feedback loops that create a biaxial coordinate system of phosphorylated histones across mitotic chromosomes. This system localizes chromosomal passenger complex (CPC) to the inner centromere, which allows its protein kinase constituent, Aurora B, to correct errors in chromosome segregation that occur in 40% of cancers. Although the CSN has been experimentally derived, the requirements of the positive feedback loops have not been examined mathematically. To gain a better understanding of the mechanisms and properties of CPC accumulation, we curated a reaction-diffusion model to capture the emergent phenomena of the CSN. The model, which included both temporal and spatial information, demonstrated the importance of a strong but balanced response between the two positive feedback loops for CPC enrichment. The proteins, Haspin, NDC80, and KNL1, were found to be essential toward this aspect of the model. Furthermore, we performed a sensitivity analysis to identify parameters that have the greatest effect on CPC enrichment. Our analysis suggests that Bub1, CPC, and Sgo1 are key modulators of the pathway while histones have little effect. This information is valuable in generating hypotheses for further experimentation and in identifying targets for drug treatment. Furthermore, the model provided evidence that the CSN alone is sufficient for significant CPC accumulation in the inner centromere.

Introduction

Aneuploidy is defined as the cellular state of having an abnormal number of chromosomes, which is observed in 40% of cancers[1]. The centromere-signaling network (CSN) is a protein signaling pathway that operates on the chromosome during mitosis to ensure accurate segregation of chromosomes and to prevent aneuploidy[2]. The CSN performs this function from a specific location on every mitotic chromosome known as the inner centromere. The inner centromere lies on the central axis between kinetochores and is identified through epigenetic mechanisms. The specification of the inner centromere requires two positive feedback loops, which are composed of a series of phosphorylation events (Fig. 1). The vertical feedback pathway results in the phosphorylation of histone, H3T3, along the vertical axis of the chromosome. This aspect of the pathway is initiated by the histone kinase, haspin, which binds to the cohesin complex that holds the two sister chromatids together down the central axis.
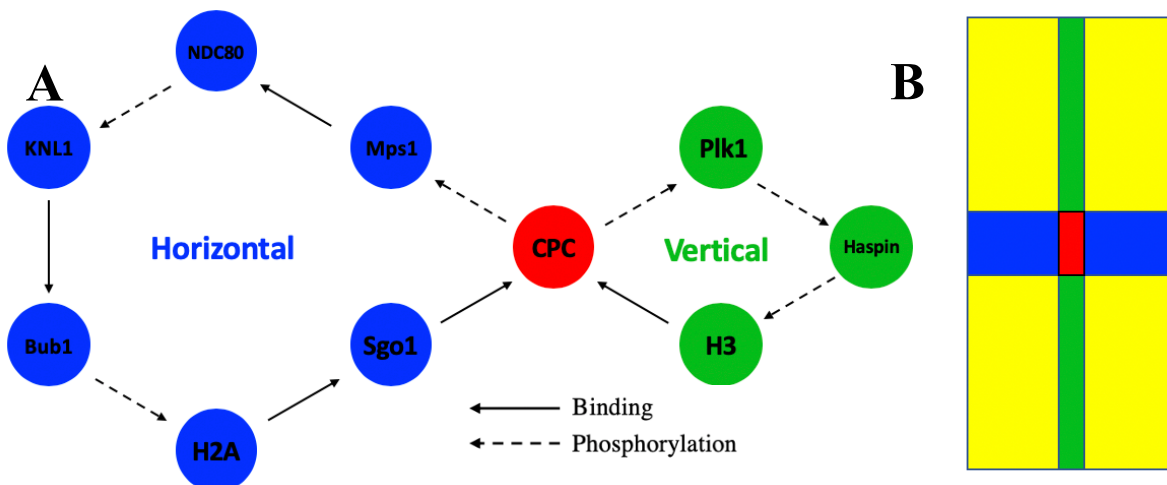

Fig. 1: The Centromere-Signaling Network Localizes CPC to the Inner Centromere. A) The CSN is composed of two positive feedback loops (A), which generate a biaxial coordinate system of phosphorylated histones across the chromosome (B). The vertical feedback pathway facilitates CPC recruitment along the vertical axis through the enrichment of haspin down the center of the chromosome. Likewise, the horizontal feedback loop creates a horizontal axis due to the localization of NDC80 and KNL1 in the kinetochores. The origin of the emergent horizontal and vertical axes resides at the inner centromere, which allows the two feedback loops to synergize and accumulate high concentrations of CPC.
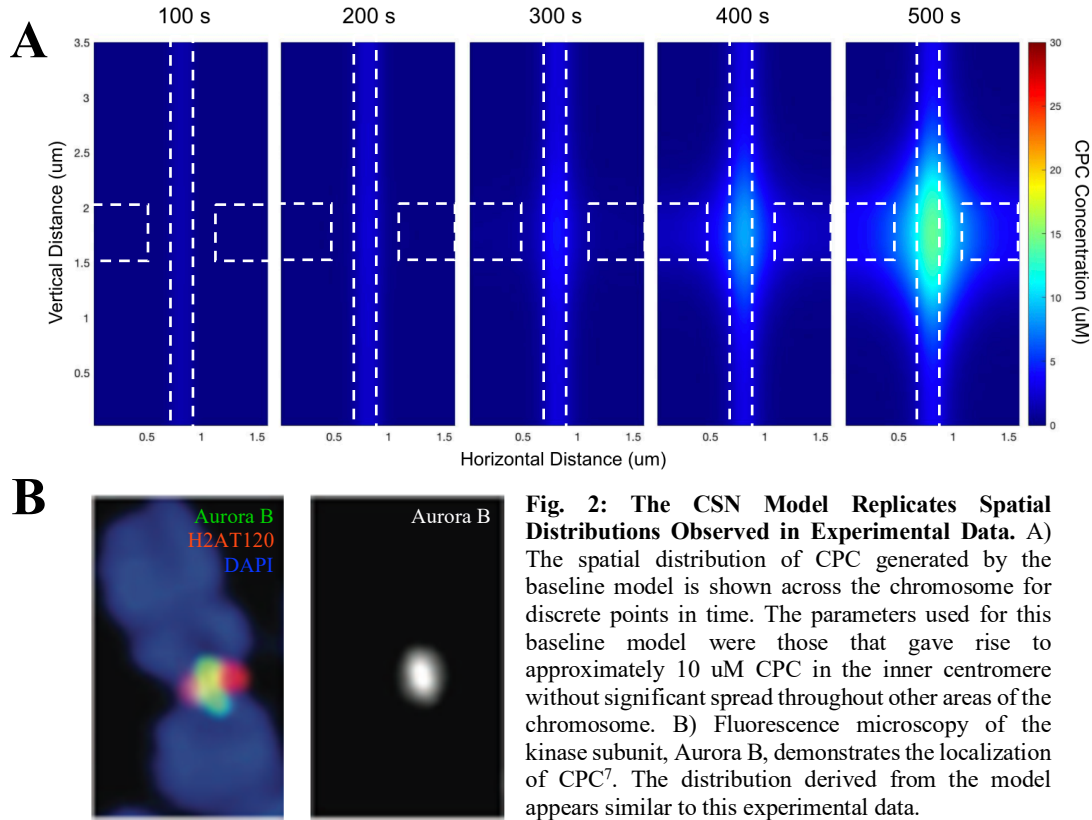
Fig. 2: The CSN Model Replicates Spatial Distributions Observed in Experimental Data. A) The spatial distribution of CPC generated by the baseline model is shown across the chromosome for discrete points in time. The parameters used for this baseline model were those that gave rise to approximately 10 uM CPC in the inner centromere without significant spread throughout other areas of the chromosome. B) Fluorescence microscopy of the kinase subunit, Aurora B, demonstrates the localization of CPC[7]. The distribution derived from the model appears similar to this experimental data.

Likewise, the horizontal feedback loop acts to phosphorylate histone, H2AT120, near the kinetochores through the localized activation of histone kinase, Bub1, creating a horizontal axis across the chromosome. These phospho-histones then recruit the protein, chromosomal passenger complex (CPC), along these axes. The emergent biaxial coordinate system acts as a biochemical bullseye, localizing high concentrations of CPC at the origin, which coincides with the inner centromere[3].

At high concentrations, CPC undergoes phase separation to form coacervates, or viscous droplets, which act as reaction crucibles by recruiting key proteins for efficient chemical reactions[4–6]. Once this accumulation occurs, a subunit of CPC, Aurora B kinase, phosphorylates kinetochore proteins to correct errors in microtubule attachments and prevent mistakes in chromosome segregation.

The purpose of modeling the CSN was to replicate the emergent spatial distribution of CPC to explore the properties and mechanisms of the pathway. To accomplish this goal, a reaction-diffusion modeling approach was employed to allow representation of both temporal and spatial aspects of the CSN. This modeling technique utilized partial differential equations to quantify protein movement and interactions over time and space. Through the resulting model, the properties of the CSN were observed and manipulated to gain a deeper understanding of the mechanisms that drive the accumulation of CPC. In particular, a computational model of the system enabled the identification of parameters toward which the network is most sensitive as well as hypothesis generation for further experimentation.

Results

Our goal was to test whether the pathways of the CSN as presented in the literature could generate a single focus of CPC at the inner centromere. This emergent property has been observed at a magnitude of approximately 10 uM in mitotic chromosomes[7]. The results of the baseline model, which was curated using experimentally measured coefficients for each enzyme, replicated this phenomenon, including the approximate magnitude expected (Fig. 2).
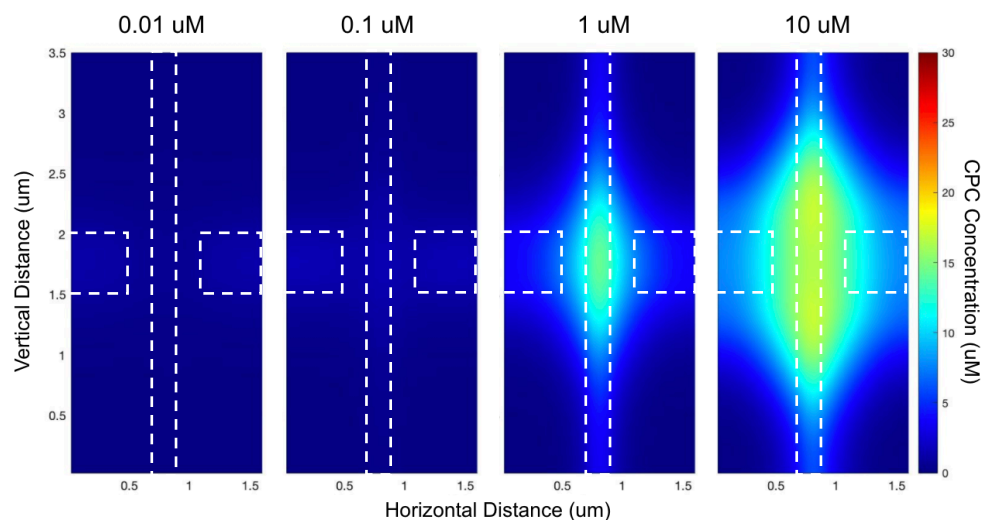
Fig. 3: Haspin Concentration is a Key Mediator of the Vertical Pathway Response. The spatial distribution of bound CPC after 500 seconds is shown for varying initial concentrations of haspin. Haspin exhibited a powerful effect on the strength of the vertical pathway response and thus the overall accumulation of CPC. At low concentrations of haspin, CPC binding was negligible, but high concentrations caused the strength of the vertical feedback response to overpower the horizontal. As a result, haspin was a good mediator of the vertical feedback loop, which was useful for balancing the CSN response in subsequent iterations of the model.

Although the separate positive feedback loops engage in crosstalk and synergize to accumulate high concentrations of CPC, each feedback pathway depends upon a separate set of molecular parameters. For example, the vertical feedback pathway was found to depend heavily upon the initial concentration of haspin. Because haspin binds to the chromosome at undetectable concentrations, this parameter was not available in the literature. As a result, the concentration of haspin was originally an unsubstantiated estimate of 1 nM. When the vertical pathway was initially modeled, it was unsuccessful in obtaining a sufficient concentration of CPC at the inner centromere. Since it was unclear how concentrated haspin must be for proper CPC recruitment, its concentration estimate was increased until the strength of the vertical and horizontal feedback responses was more balanced (Fig. 3). When adding steps or modifying reactions in subsequent stages of the model, imbalances between the CPC concentrations on the horizontal and vertical axes were tuned using the concentration of haspin due to its large effect on the vertical feedback response. The optimal concentration estimate of haspin was determined to be 1 uM since it generated the expected magnitude of CPC at the inner centromere and higher concentrations
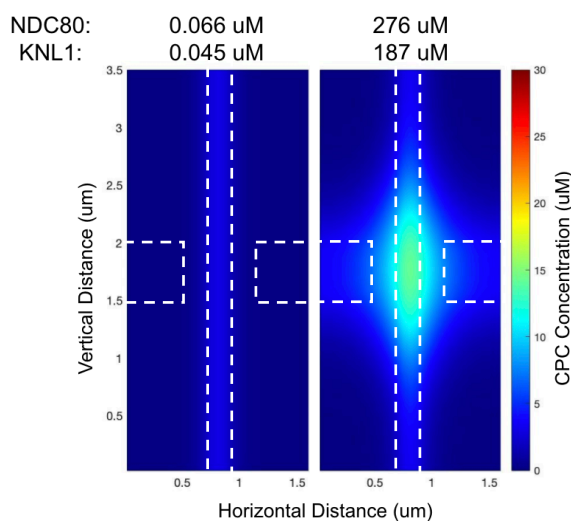

Fig. 4: Enriched Kinetochore Protein Concentrations are Important for the Horizontal Pathway Response. The spatial distribution of bound CPC after 500 seconds is shown for both whole cell and enriched concentration estimates of the kinetochore proteins, NDC80 and KNL1. The average concentrations of these proteins across the whole cell were small, which gave rise to negligible accumulation of bound CPC. When the concentrations were adjusted for enrichment at the kinetochores, the appropriate spatial distribution of CPC emerged. The strong effect of NDC80 and KNL1 on CPC binding suggests that these proteins are important for facilitating the response of the horizontal feedback loop.
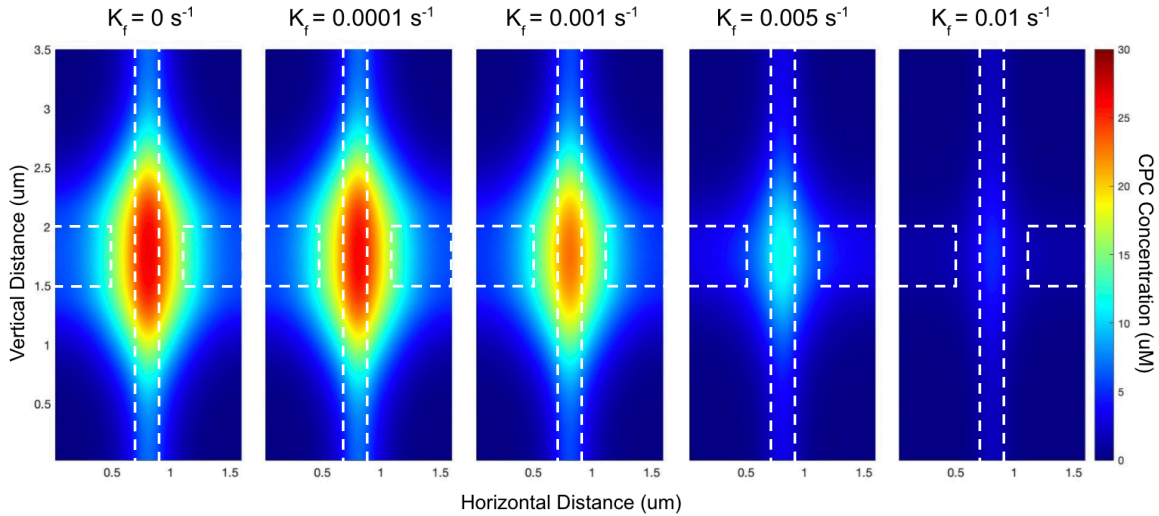
3

Fig. 5: Phosphatases Generate a Contained Peak of CPC in the Inner Centromere. The spatial distribution of bound CPC after 500 seconds is shown for varying ubiquitous forward rates of phosphatases. For low rates of phosphatase action, CPC binding occurred outside of the inner centromere. At high forward rates, phosphatases diminished CPC binding within the inner centromere. A reaction rate of 0.005 s^{-1} generated the most balanced response with a well-defined peak of CPC at the center of the chromosome.

caused the vertical response to overpower the horizontal.

Like the vertical feedback pathway, the horizontal portion of the CSN accumulated negligible CPC concentrations in initial iterations of the model. The failure of the pathway to facilitate CPC binding to the chromosome was attributed to the low concentrations of kinetochore proteins involved in the horizontal pathway, specifically NDC80 and KNL1 (Fig. 4). The original estimated concentrations of 0.066 and 0.045 uM, respectively, were whole cell measurements, or averages across the entire volume of the cell. However, these proteins are localized within the much smaller volume of the kinetochores, where their concentrations are highly enriched. Using the estimated volume ratio of a kinetochore to the average cell, the enriched concentrations were calculated at 276 and 187 uM. With these modifications, a substantial accumulation of CPC was observed along the horizontal axis. Given the strong effect of NDC80 and KNL1 concentrations on CPC binding, it was determined that these species are important for driving the horizontal pathway response.

Once the vertical and horizontal feedback responses were balanced, phosphatases were implemented to add physiological accuracy and diminish CPC accumulation outside of the inner centromere. These general phosphatases were modeled as simple, first-order reverse reactions added to each phosphorylation reaction (Fig. 1A). The uniform forward rate for all phosphatases was iteratively increased to determine the most appropriate value (Fig. 5). If the rate was too small, the phosphatases were unable to quench CPC accumulation outside of the inner centromere. When the rate grew too large, the concentration of CPC within the inner centromere began to decrease. The most balanced model had a forward rate of 0.005 s^{-1}. This value was supported by experimental data on the phosphatase for histone, H3T3, which exhibited a forward rate of approximately 0.005 s^{-1} as well[8,9].

A ubiquitous diffusion constant was also defined for all mobile proteins after difficulties in obtaining appropriate measurements from experimental data. The process of estimating an appropriate rate of diffusion revealed that the diffusion constants of most proteins had a negligible effect on both the magnitude and spatial distribution of CPC recruitment. The exception to this observation was the diffusivity of CPC bound either to H3T3, H2AT120, or both (Fig. 6). The model required a non-zero diffusion for bound CPC to allow it to spatially interact with its substrates, Plk1 and Mps1. This diffusivity can be physiologically justified since Aurora B kinase has the ability to move

dynamically about on a tether formed by INCENP, another subunit of CPC[10]. As expected, a smaller diffusion constant for bound CPC generated a peak of CPC at the inner centromere, which may be indicative of the effects of coacervate formation. Because of the viscous environment created within a CPC coacervate, diffusion is greatly reduced[4]. Combined with the ability of CPC coacervates to recruit CPC more rapidly, this reduced diffusivity facilitates CPC localization by maintaining CPC in the inner centromere and preventing its spread along the chromosome.
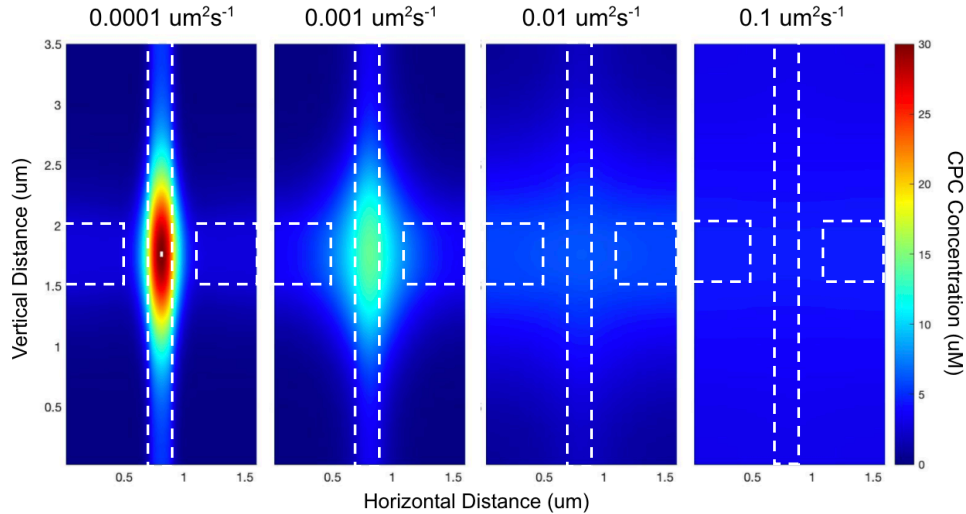

Fig. 6: The Sensitivity of CPC Diffusion Indicates the Importance of Coacervates. The spatial distribution of bound CPC after 500 seconds is shown for varying diffusion constants of the three CPC subspecies. The small diffusivity given to bound CPC represents the ability of the Aurora B kinase subunit to move about on the arm-like INCENP subunit. Intuitively, slower movement of the kinase created a more defined inner centromere peak. This emergent phenomenon supports the hypothesis that coacervates, which limit the diffusivity of constituent molecules, facilitate the localization of CPC. The diffusion constant selected for the baseline model, 0.001 um^{2}s^{-1}, was the value that balanced negligible CPC binding with the spread of CPC outside of the inner centromere.
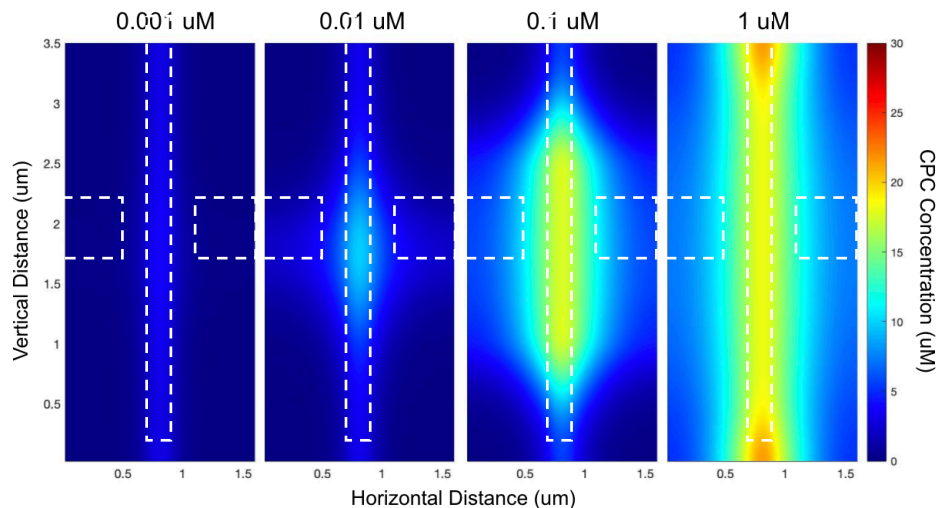

Fig. 7: Bub1 Concentration Affects the Balance Between Vertical and Horizontal Response. The spatial distribution of bound CPC after 500 seconds is shown for varying initial concentrations of Bub1. Even though Bub1 is a component of the horizontal feedback loop, increasing values of its initial concentration created high concentrations of CPC along the vertical axis. It is suspected that the balance between the vertical and horizontal pathways was altered due to the increase in Bub1 concentration, allowing the vertical response to dominate.

5

To determine which parameters have the greatest effect on CPC localization, parameter sweeps were performed on the finalized model. Overall, the model was not very robust to most changes, causing some interesting phenomena to emerge. One such result was the effect of perturbing the K_{cat} of Bub1 phosphorylation, which is a protein kinase in the horizontal feedback loop. Like all other phosphorylations, increasing values of K_{cat} generated higher concentrations of CPC across the chromosome (Fig. 7). Likewise, increasing Bub1 concentrations also increased CPC binding to the chromosome. However, despite its role in the horizontal pathway, Bub1 concentration and phosphorylation rate unintuitively increased the CPC response along the vertical axis. The hypothesized explanation for this phenomenon is that changes in the horizontal pathway affect the balance between the responses of the two feedback loops, allowing the vertical axis to dominate.

Another unexpected result of the parameter sweeps was that changes in the parameters dictating histone phosphorylation did not noticeably affect CPC concentrations (Fig. S3). These results suggest that the spatial location of the histone code matters much more than the parameters that govern its phosphorylation. This finding also has implications in future drug targeting of the pathway. When attempting to modulate the function of the CSN, it may not be effective to target haspin or Bub1, which are the kinases involved in the phosphorylation of H3T3 and H2AT120, respectively. Other protein targets may be more effective in this regard.

One of the proteins that strongly affects CPC binding is Sgo1 even though it is not a limiting reagent in the horizontal pathway. Although the concentration of Sgo1 is clamped throughout the simulation so that it cannot be depleted, changes in this clamped concentration have a strong impact on the accumulation of CPC (Fig. 8). Less surprisingly, the clamped concentration of free CPC was found to be a sensitive parameter as well. With both of these proteins, an increase in concentration caused higher rates of binding with histones, thus pushing the positive feedback loops forward. Furthermore, the dissociation constants for CPC
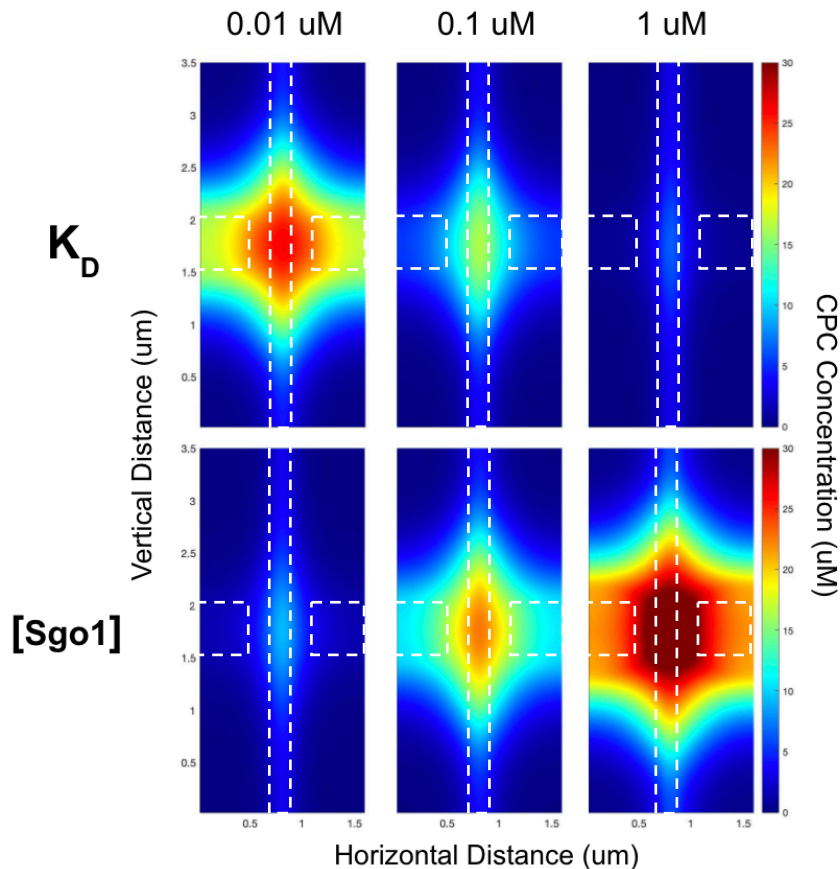

Fig. 8: Sgo1 Binding is a Sensitive Step in the CSN. The spatial distribution of bound CPC after 500 seconds is shown for varying dissociations constants of Sgo1 binding to H2AT120 (top) as well as a range of Sgo1 concentrations (bottom). Lower dissociation constants, which indicate higher affinities, increased CPC binding by pushing forward the Sgo1 binding reaction. Increasing the clamped concentration of Sgo1 was another method of facilitating its binding to H2AT120, which also accelerated the positive feedback mechanisms. As a result, Sgo1 was identified as a sensitive component of the CSN.

and Sgo1 binding had a strong impact on CPC accumulation since higher affinities also tend to increase the rate of the binding reactions (Fig. 7). In fact, small dissociation constants for CPC binding strengthened the response along the horizontal axis more than the vertical. This phenomenon allowed CPC to localize at the kinetochores, which may enable it to better phosphorylate and correct errors in microtubule attachment. For both the concentrations and dissociation constants of free CPC and Sgo1, parameter sweeps identified the orders of magnitude for which the model output was most balanced. At low concentrations and high dissociation constants, CPC recruitment was not strong enough to generate the biaxial coordinate system and thus a peak at the inner centromere. For high concentrations and low dissociation constants, CPC binding occurred strongly in areas outside of the vertical and horizontal axes. The balance between these two extremes occurred around the concentration and kinetic parameters that had previously been defined for free CPC and Sgo1, which verified the accuracy of these parameters. However, the large effect of perturbations on these molecules indicate their important role in CPC recruitment. As a result, these proteins would be prime targets for modulating the network in future experimentation.

Discussion

Overall, modeling the CSN provided an insight into the specific properties and mechanisms of the signaling pathway. Tuning the network structure and parameters to obtain the expected spatial distribution of CPC revealed the aspects of the pathway that are most important for its function. For example, generating a strong but balanced vertical and horizontal pathway response depended heavily upon haspin, NDC80, and KNL1 concentrations but not on histone phosphorylation rates. Sgo1 and free CPC binding were also identified as sensitive parameters in the signaling pathway. These findings give rise to potential *in vitro* experiments for further validation.

By proving that the CSN alone is sufficient to accumulate CPC at the inner centromere, the model serves as evidence in a long-standing debate over whether other cellular mechanisms are necessary for CPC recruitment. It has been suggested that other signaling mechanisms play a large role in the ability of CPC to robustly phosphorylate kinetochores under certain conditions[11,12]. Despite the sensitivity of the CSN compared to these robust mechanisms, the model provides preliminary evidence that no other proteins are required for CPC localization. To further address this issue, microtubule interactions could be added to the model in future versions. If, after adding this new component, the binding of CPC has not changed significantly, the model would provide even stronger evidence that the CSN is sufficient for CPC accumulation.

Although the model has already proved useful in illuminating the properties of the CSN, there is much more complexity that could be added to improve its biological accuracy. One possibility is the addition of phase separation above a critical concentration of CPC. This aspect of the CSN was omitted for simplicity but would greatly heighten the predictive abilities of the model. It is suspected that coacervate formation would increase CPC recruitment to the inner centromere, creating a sharper and more stable peak relative to the concentrations along the vertical and horizontal axes. Autophosphorylation is also an important component of the pathway that was previously excluded. Mps1, Bub1, and CPC all undergo activation through autophosphorylation upon binding to stationary proteins. Modeling these activations would greatly increase the biological relevance of the model. Finally, experiments to test the parameters and properties observed in the model would be valuable in validating its usefulness for further hypothesis generation.

Given the outputs of the model, it would be interesting to either simulate or experimentally test the effects of protein overexpression. It is suspected that the resulting concentration imbalances would give rise to aneuploidy through malfunction of the CSN[13–17]. By applying initial concentrations from cancer to the model, predictions about the robustness of the network during disease states could be assembled. Following experimental verification of the outcomes, the data could be used in the development of targeted treatments for cancer.

Methods

Model Structure

The first step in curating a model of the CSN was to thoroughly establish all of the relevant molecular interactions. The vertical feedback pathway begins with CPC phosphorylation of Plk1, which then phosphorylates haspin[18,19]. Haspin, which is localized along the vertical axis of the chromosome, phosphorylates histone H3T3 to allow it to bind free CPC[18,20]. On the horizontal portion of the pathway, active CPC phosphorylates Mps1. Phosphorylated Mps1 then binds to the kinetochore protein, NDC80, where it autophosphorylates on a different site[21,22]. The dynamically bound and activated Mps1 can then phosphorylate a different kinetochore protein, KNL1, which allows Bub1 to bind and autophosphorylate[23]. The activated Bub1 dissociates to phosphorylate histone H2AT120. Sgo1 can then bind H2AT120, which allows CPC to bind to the complex as well. Once CPC binds to one or both histones, it undergoes autophosphorylation to activate its kinase activity and continue the positive feedback.

The open source software, Virtual Cell (VCell), was used for modeling the CSN due to its ability to implement reaction-diffusion modeling through a simple user interface[24]. VCell provided the capability to create both mass action binding reactions and Michaelis-Menten catalysis for phosphorylation reactions (Fig. S1). The parameters required for Michaelis-Menten reactions were K_m and V_{max}. Because K_m and K_{cat} were the values more commonly defined in the literature, V_{max} was specified as the product of K_{cat} and the concentration of the catalyst as a function of time. Mass action kinetics required both forward and reverse reaction rates, which were also difficult to identify from past experimentation. As a result, a general estimate designating a K_f of 1 s^{-1}uM^{-1} and K_D of 0.15 uM was applied to all binding reactions except CPC binding. The reverse reaction rate was the product of these two values. Parameter sweeps revealed that changes in K_f had a negligible effect on model output. For CPC binding, all properties were the same except that a K_D of 2 uM was applied.

Bound CPC consisted of three subspecies, which were summed to obtain the total concentration of CPC. Two of the subspecies were bound to either H3T3 or H2AT120, and the final CPC subspecies was bound to both histones. In original versions of the model, the binding of doubly bound CPC was modeled using a one step reaction, which represented simultaneous binding to both histones. Because this reaction occurred very slowly, this model structure did not generate a high concentration ratio of CPC at the inner centromere to CPC on the vertical or horizontal axes. To alleviate this oversight, double binding of CPC was split into two sequential paths, binding first to one histone and then to the other. The new reaction structure produced a sharper peak of CPC at the inner centromere as expected.

Another reaction structure that was refined throughout different versions of the model was the activation of Bub1. Physiologically, Bub1 binds to KNL1 where it undergoes autophosphorylation, subsequently dissociating to phosphorylate histone H2AT120. Since auto-activations were omitted from the current version of the model, different methods were tested to obtain an acceptable model output. The first attempt modeled the series of steps as a simple binding reaction, which effectively assumed that Bub1 automatically activated upon binding with KNL1. Although this reaction structure produced the desired accumulation of CPC at the inner centromere, the peak was not stable over time. The reaction was modified to regenerate KNL1 after Bub1 dissociation, which was not included in the previous reaction. The resulting peak of CPC concentration remained stable over time, but the magnitude was drastically reduced to 1.5 uM at the inner centromere. The final version of the model utilized a Michaelis-Menten reaction in which KNL1 directly facilitated the autophosphorylation of Bub1. Since Bub1 is only transiently bound to KNL1, the reaction sufficed as a simplified representation of the steps for Bub1 activation. The binding affinity between KNL1 and Bub1 was reflected in the K_m value while K_{cat} represented the rate of Bub1 autophosphorylation. The resulting peak of CPC was stable and reached a sufficient magnitude of approximately 10 uM (Fig. 2).

Before the entire CSN was implemented in the model, each positive feedback loop was modeled separately to ensure that they individually generated their respective coordinate axes. Each model began as a non-spatial representation of the protein species over time. Non-spatial simulations used a fifth order Runge-Kutta-Fehlberg PDE solver with variable time steps between 10^{-8} and 10 seconds. Using these simulations, preliminary parameter sweeps were performed to identify errors within the pathway and determine which parameters caused the largest changes in model output. The parameters that were most sensitive to perturbations required more accurate estimates. Once these parameters were addressed, the spatial component of the model was added. In spatial simulations, a regular grid fully-implicit finite volume PDE solver with variable time steps was implemented. The maximum time step as well as the output interval was set to 10 seconds for the duration of the 500 seconds spanned by the model. The total concentration of bound CPC in spatial simulations tended to be less than that generated by non-spatial simulations since the diffusion of certain proteins was restricted by the geometry of the chromosome.

Model Geometry

Because sister chromatids are fused together by cohesin during the stage of mitosis in which the CSN is active, the geometry of the model was simplified to a 1.6 by 3.2 um rectangle (Fig. S2). The kinetochores were represented as two squares of dimension 500 nM on the border of the chromosome. The vertical axis was defined as an area down the center of the chromosome with a width of 200 nM. Haspin is recruited to this axis by a topoisomerase before the time period captured by the model. To simulate this distribution, haspin was restricted to the vertical axis by multiplying its initial concentration and diffusion coefficient with the Boolean logic statement, $(x > 0.7)$ && $(x < 0.9)$, where x is the horizontal distance across the chromosome. NDC80 and KNL1 were constrained to the kinetochores using the same method. Although VCell was capable of creating compartmental geometries, the Boolean approach simplified the reaction diagram and decreased the runtime of simulations.

Model Parameters

Many of the model parameters were gleaned from established literature, although some, such as haspin concentration and mass action kinetics, were estimated based on previous knowledge or parameter sweeps (Fig. S2). Most initial concentrations were derived from quantitative proteomic measurements of Xenopus laevis frog eggs[25]. Since CSN proteins are likely upregulated in the mitotic egg, the concentrations were assumed to be the upper bound of concentrations found in human cells. These measurements were also whole cell averages of the protein concentrations, which necessitated the use of volume ratios to obtain enriched concentrations for localized proteins. For example, the Xenopus concentrations of NDC80 and KNL1, 0.066 and 0.045 uM, respectively, were modified to determine the kinetochore concentrations. To obtain the volume ratio for this adjustment, the average cell was assumed to be a sphere with a radius of 5 um, and the kinetochores were approximated as cubes of dimension 500 nm. In addition, the Xenopus measurements of Plk1 and Mps1 were modified in order to initiate the feedback loops of the CSN. For both of these kinases, 80% of the total concentration was initially unphosphorylated while the remaining 20% was automatically activated.

For Bub1, Mps1, Plk1, Sgo1, and free CPC, the concentrations were clamped for the duration of the simulation. Because the volume of the simulated chromosome was very small compared to the rest of the cell, these protein concentrations should not be depleted by the action of the CSN. Clamping the protein concentrations throughout the simulation replicated the cytoplasmic pool and prevented depletion of these species. When left unclamped, these proteins became the limiting reagents of the CSN, resulting in negligible concentrations of CPC on the order of 0.001 uM or less. One ramification of clamping species in VCell was that the proteins were automatically assumed to be well-mixed. As a result, no diffusion constants were required for these species.

For the immobilized protein species, which included NDC80, KNL1, and histones, the diffusion constant was kept at zero. Other proteins, such as bound CPC, haspin, and

activated Mps1, were given small diffusivities despite their bound state to the chromosome. However, the latter two were restricted to the vertical axis and kinetochores, respectively, using Boolean logic statements. These non-zero diffusion constants were required for VCell to recognize the ability of two species to spatially interact, but the diffusivities were not physiologically unfounded. On the contrary, the diffusion constants represent the biological phenomenon in which the kinases in question have restricted movement on the end of an arm-like protein subunit.

Multiple methods were attempted to obtain the diffusion coefficients for the remaining protein species. The first effort involved calculating the protein radius from its molecular weight, which was then used in the Stokes-Einstein equation to obtain diffusivities on the order of 100 um^2s^{-1}. When implemented in the model, the resulting values were found to be much too large to create a defined biaxial coordinate system. A second attempt at calculating diffusivities used experimental data to determine the diffusivity of CPC as well as a ratio of cytoplasmic to coacervate diffusivities[4]. The values produced by this method were on the order of 0.1 um^2s^{-1}. While these estimates produced much better results from the model, the diffusion constants were later decreased to a uniform 0.001 um^2s^{-1} to obtain a more defined spatial distribution of CPC.

All of the Michaelis-Menten parameters were found in the literature on the relevant kinases. For example, the phosphorylation of Plk1 and Mps1 was defined by the parameters describing Aurora B kinase, which is a component of CPC. With some kinases, the parameters for the specific substrate interaction were not available in the literature, in which case the phosphorylation of a similar substrate was used as a substitute. One instance of this was haspin phosphorylation mediated by the catalyst, Plk1. In this case, it was imperative that the parameters be derived from a substrate with comparable affinity to Plk1 due the POLO-Box domain interaction between the kinase and haspin[26].

References

1. Gordon, D. J., Resio, B. & Pellman, D. Causes and consequences of aneuploidy in cancer. *Nat. Rev. Genet.* **13**, 189–203 (2012).
2. Knowlton, A. L., Lan, W. & Stukenberg, P. T. Aurora B Is Enriched at Merotelic Attachment Sites, Where It Regulates MCAK. *Curr. Biol.* **16**, 1705–1710 (2006).
3. Trivedi, P. & Stukenberg, P. T. A Centromere-Signaling Network Underlies the Coordination among Mitotic Events. *Trends Biochem. Sci.* **41**, 160–174 (2016).
4. Trivedi, P. *et al.* The inner centromere is a biomolecular condensate scaffolded by the chromosomal passenger complex. *Nat. Cell Biol.* **21**, 1127–1137 (2019).
5. Shin, Y. & Brangwynne, C. P. Liquid phase condensation in cell physiology and disease. *Science* **357**, (2017).
6. Banani, S. F., Lee, H. O., Hyman, A. A. & Rosen, M. K. Biomolecular condensates: organizers of cellular biochemistry. *Nat. Rev. Mol. Cell Biol.* **18**, 285–298 (2017).
7. Yamagishi, Y., Honda, T., Tanno, Y. & Watanabe, Y. Two Histone Marks Establish the Inner Centromere and Chromosome Bi-Orientation. *Science* **330**, 239–243 (2010).
8. Qian, J., Lesage, B., Beullens, M., Van Eynde, A. & Bollen, M. PP1/Repo-Man Dephosphorylates Mitotic Histone H3 at T3 and Regulates Chromosomal Aurora B Targeting. *Curr. Biol.* **21**, 766–773 (2011).
9. Zhang, L. & Lee, E. Y. C. Mutational Analysis of Substrate Recognition by Protein Phosphatase 1. *Biochemistry* **36**, 8209–8214 (1997).
10. van der Horst, A. *et al.* Inter-domain Cooperation in INCENP Promotes Aurora B Relocation from Centromeres to Microtubules. *Cell Rep.* **12**, 380–387 (2015).
11. Hindriksen, S., Lens, S. M. A. & Hadders, M. A. The Ins and Outs of Aurora B Inner

Centromere Localization. *Front. Cell Dev. Biol.* **5**, (2017).

12. Broad, A. J., DeLuca, K. F. & DeLuca, J. G. Aurora B kinase is recruited to multiple discrete kinetochore and centromere regions in human cells. *J. Cell Biol.* **219**, (2020).

13. Ricke, R. M., Jeganathan, K. B. & van Deursen, J. M. Bub1 overexpression induces aneuploidy and tumor formation through Aurora B kinase hyperactivation. *J. Cell Biol.* **193**, 1049–1064 (2011).

14. Mu, J., Fan, L., Liu, D. & Zhu, D. Overexpression of shugoshin1 predicts a poor prognosis for prostate cancer and promotes metastasis by affecting epithelial–mesenchymal transition. *OncoTargets Ther.* **12**, 1111–1118 (2019).

15. Kim, J.-E. *et al.* Coumestrol Epigenetically Suppresses Cancer Cell Proliferation: Coumestrol Is a Natural Haspin Kinase Inhibitor. *Int. J. Mol. Sci.* **18**, (2017).

16. González-Loyola, A. *et al.* Aurora B Overexpression Causes Aneuploidy and p21Cip1 Repression during Tumor Development. *Mol. Cell. Biol.* **35**, 3566–3578 (2015).

17. Ling, Y. *et al.* Overexpression of Mps1 in colon cancer cells attenuates the spindle assembly checkpoint and increases aneuploidy. *Biochem. Biophys. Res. Commun.* **450**, 1690–1695 (2014).

18. Zhou, L., Tian, X., Zhu, C., Wang, F. & Higgins, J. M. Polo-like kinase-1 triggers histone phosphorylation by Haspin in mitosis. *EMBO Rep.* **15**, 273–281 (2014).

19. Moutinho-Santos, T. & Maiato, H. Plk1 puts a (Has)pin on the mitotic histone code. *EMBO Rep.* **15**, 203–204 (2014).

20. Wang, F. *et al.* Histone H3 Thr-3 Phosphorylation by Haspin Positions Aurora B at Centromeres in Mitosis. *Science* **330**, 231–235 (2010).

21. Nilsson, J. Mps1-Ndc80: one interaction to rule them all. *Oncotarget* **6**, 16822–16823 (2015).

22. McCleland, M. L. *et al.* The highly conserved Ndc80 complex is required for kinetochore assembly, chromosome congression, and spindle checkpoint activity. *Genes Dev.* **17**, 101–114 (2003).

23. Breit, C. *et al.* Role of Intrinsic and Extrinsic Factors in the Regulation of the Mitotic Checkpoint Kinase Bub1. *PLOS ONE* **10**, e0144673 (2015).

24. Loew, L. M. & Schaff, J. C. The Virtual Cell: a software environment for computational cell biology. *Trends Biotechnol.* **19**, 401–406 (2001).

25. Wühr, M. *et al.* Deep Proteomics of the Xenopus laevis Egg using an mRNA-derived Reference Database. *Curr. Biol. CB* **24**, 1467–1475 (2014).

26. Elia, A. E. H. *et al.* The Molecular Basis for Phosphodependent Substrate Targeting and Regulation of Plks by the Polo-Box Domain. *Cell* **115**, 83–95 (2003).
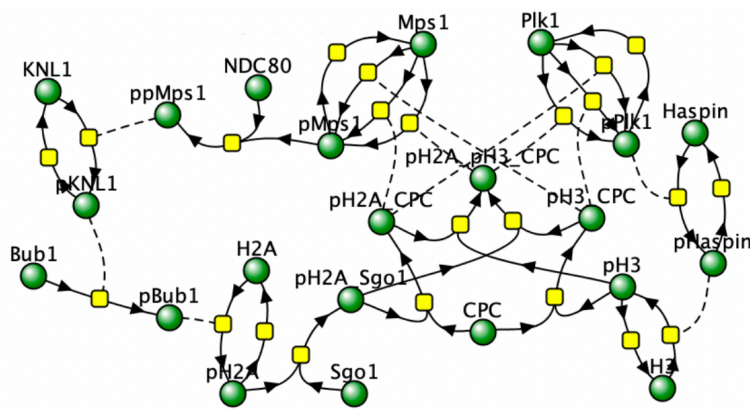
Supplemental

Fig. S1: Virtual Cell Reaction Diagram. The structure of the CSN as implemented in VCell exemplifies the highly complex nature of the pathway. Green circles represent protein species, yellow boxes indicate individual reactions, and dashed lines denote enzyme catalysis. First order phosphatase reactions added reversibility to all phosphorylation reactions. The three subspecies of CPC, which are designated pH2A_CPC, pH3_CPC, and pH2A_pH3_CPC, were summed for the total concentration of bound CPC. The presence of the different CPC subtypes required three identical phosphorylation reactions for Mps1 and Plk1 to allow each subspecies to catalyze the reactions.

Protein	Initial Conc (uM)	Diffusivity (um²/s)	Phosphorylation	K_m (uM)	K_{cat} (s⁻¹)
Bub1	- 0.02 -	--	Haspin	79	12
pBub1	0	0.001	H2A	41.1	1.52
CPC	- 0.12 -	--	H3	0.058	0.467
pH3-CPC	0	0.001	KNL1	74	1.58
pH2A-Sgo1-CPC	0	0.001	Mps1	14.2	1.11
pH2A-Sgo1-pH3-CPC	0	0.001	Plk1	14.2	1.11
Haspin	^ 1 ^	^ 0.001 ^			
pHaspin	0	^ 0.001 ^	**Binding**	K_D (uM)	K_f (s⁻¹uM⁻¹)
H2A	340	0	CPC-histone	2	1
pH2A	0	0	Other	0.15	1
H3	340	0			
pH3	0	0			
KNL1	* 187 *	0			
pKNL1	0	0			
Mps1	- 0.07 -	--			
pMps1	0.02	0.001			
ppMps1	0	* 0.001 *			
NDC80	* 276 *	0			
Plk1	- 0.19 -	--			
pPlk1	0.05	0.001			
Sgo1	- 0.03 -	--			
pH2A-Sgo1	0	0			

Chromosome
Vertical Axis
Kinetochores

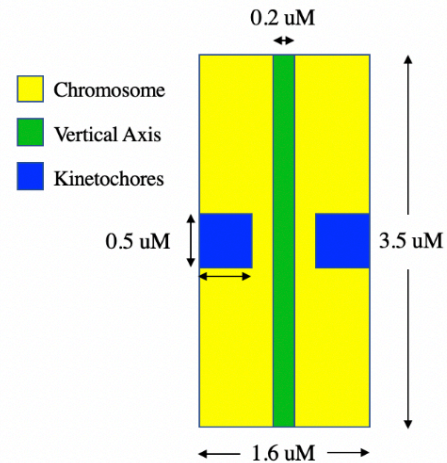0.2 uM
0.5 uM
3.5 uM
1.6 uM

Fig. S2: Model Parameters and Geometry. Kinetic constants for both Michaelis-Menten and mass action reactions are displayed on the upper right. The initial concentrations and diffusion coefficients of each protein are given in the leftmost table. Concentrations surrounded by "- -" are clamped at their initial value throughout the simulation, and the concentrations of these species are automatically assumed to be well-mixed, negating the need for diffusion coefficients. Parameters denoted by "* *" or "^ ^" are localized to the kinetochores or vertical axis, respectively, using Boolean logic statements. The compartmental specifications are shown in the geometric diagram of the chromosome.
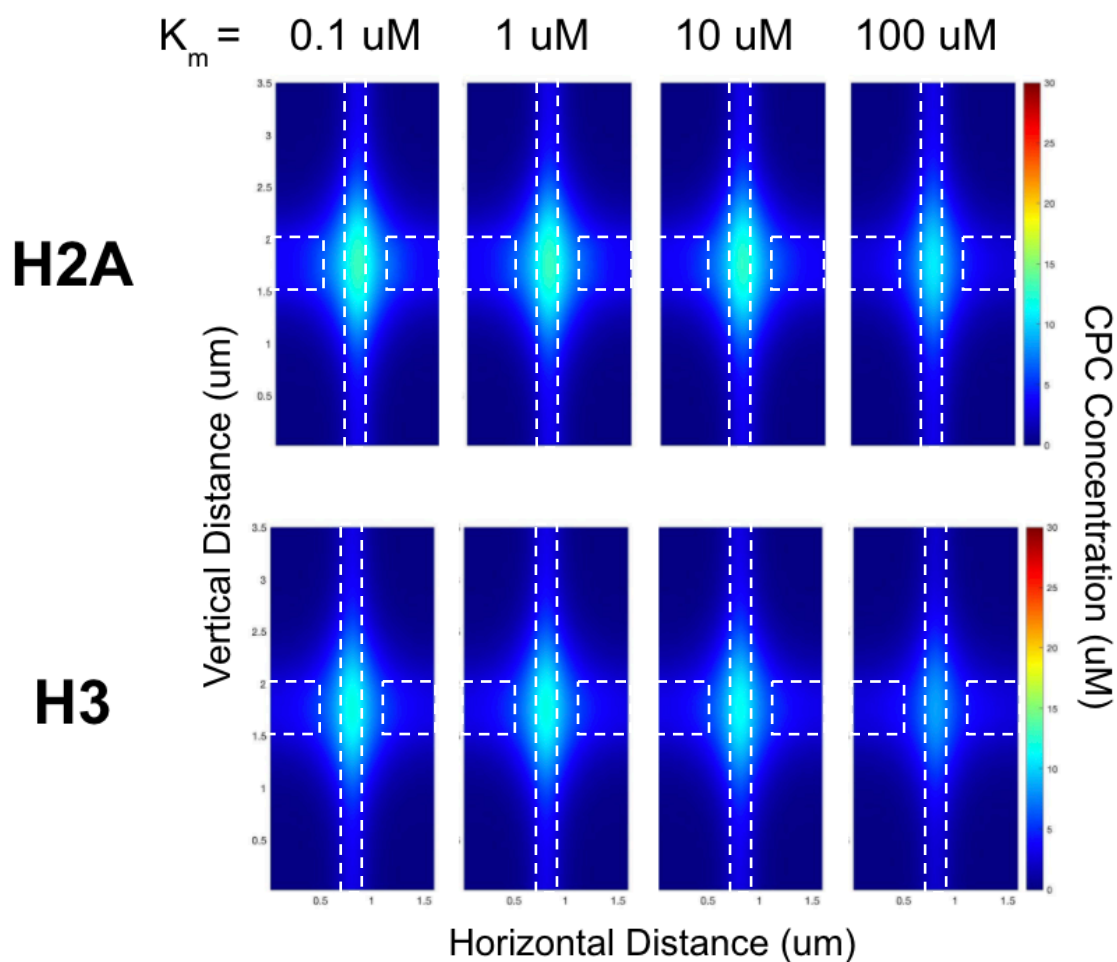
12

Fig. S3: Histone Phosphorylation is Robust to Parameter Changes. The spatial distribution of bound CPC after 500 seconds is shown for varying Km values of histone phosphorylation. Neither H3T3 nor H2AT120 phosphorylation parameters had a large effect on the emergent distribution of CPC binding. This result suggests that while the location of histone phosphorylation is a key contributor to the distribution of CPC, the parameters governing this reaction are not.